

Enzyme Chemistry

How to cite: *Angew. Chem. Int. Ed.* **2021**, *60*, 14188–14194

International Edition: doi.org/10.1002/anie.202104372

German Edition: doi.org/10.1002/ange.202104372

Structural and Mechanistic Insights into C–S Bond Formation in Gliotoxin

Kirstin Scherlach, Wolfgang Kutenlochner, Daniel H. Scharf, Axel A. Brakhage, Christian Hertweck, Michael Groll, and Eva M. Huber*

Abstract: *Glutathione-S-transferases (GSTs) usually detoxify xenobiotics. The human pathogenic fungus *Aspergillus fumigatus* however uses the exceptional GST GliG to incorporate two sulfur atoms into its virulence factor gliotoxin. Because these sulfurs are essential for biological activity, glutathionylation is a key step of gliotoxin biosynthesis. Yet, the mechanism of carbon–sulfur linkage formation from a bis-hydroxylated precursor is unresolved. Here, we report structures of GliG with glutathione (GSH) and its reaction product cyclo[*L*-Phe-*L*-Ser]-bis-glutathione, which has been purified from a genetically modified *A. fumigatus* strain. The structures argue for stepwise processing of first the Phe and second the Ser moiety. Enzyme-mediated dehydration of the substrate activates GSH and a helix dipole stabilizes the resulting anion via a water molecule for the nucleophilic attack. Activity assays with mutants validate the interactions of GliG with the ligands and enrich our knowledge about enzymatic C–S bond formation in gliotoxin and epipolythiodioxopiperazine (ETP) natural compounds in general.*

Introduction

Infections with the airborne mold *Aspergillus fumigatus* are a major cause of death in immunocompromised patients.^[1] To set the ground for the development of diagnostic tools and novel therapeutic agents for invasive aspergillosis, a detailed understanding of the pathogenicity mechanisms of *A. fumigatus* is required. The most prominent virulence factor of *A. fumigatus* is gliotoxin,^[2] a secondary metabolite belonging to the class of epipolythiodioxopiperazine (ETP) compounds.^[3] ETPs are hallmarked by a pharmacophoric, trans-

annular disulfide bridge and a diketopiperazine (DKP) core structure that originates from the condensation of two amino acids.^[4] The DKP scaffold of gliotoxin is assembled from the two amino acids *L*-Phe and *L*-Ser by the action of the non-ribosomal peptide synthetase GliP.^[5] According to the current model, hydroxylation of both C_α atoms of the cyclo[*L*-Phe-*L*-Ser] dipeptide by the cytochrome P450 monooxygenase GliC is followed by spontaneous water elimination and the glutathione-S-transferase (GST) GliG transfers two molecules of reduced glutathione (GSH, γ -Glu-Cys-Gly; Figure 1).^[6] Successive decomposition of the GSH moieties creates free thiol groups that are oxidized by the oxidoreductase GliT to the epidithio bridge.^[7] The latter structural motif is essential for the biological activity of gliotoxin by mediating redox cycling, protein conjugation and the formation of reactive oxygen species.^[8] Despite the key function of the sulfur atoms in gliotoxin, the mechanistic details of sulfur incorporation and carbon–sulfur bond formation by GliG are not yet elucidated. Here we report crystal structures of GliG in apo, substrate and product bound states that in conjunction with activity assays identify key residues for ligand binding and substrate conversion during gliotoxin biosynthesis.

Results and Discussion

GliG from *A. fumigatus* was heterologously expressed in *Escherichia coli* and the protein was purified by affinity and size exclusion chromatography (Figures S1 and S2A in the Supporting Information). Like other GSTs,^[9] GliG forms a homodimer in solution (Figure S3A in the Supporting

[*] W. Kutenlochner, Prof. Dr. M. Groll, Dr. E. M. Huber
Technical University of Munich
Center for Protein Assemblies
Ernst-Otto-Fischer-Strasse 8, 85747 Garching (Germany)
E-mail: eva.huber@tum.de

Dr. K. Scherlach, Prof. Dr. C. Hertweck
Department of Biomolecular Chemistry
Leibniz Institute for Natural Product Research and Infection Biology (HKI)
Beutenbergstrasse 11a, 07745 Jena (Germany)

Dr. D. H. Scharf, Prof. Dr. A. A. Brakhage
Department of Molecular and Applied Microbiology
Leibniz Institute for Natural Product Research and Infection Biology (HKI)
Beutenbergstrasse 11a, 07745 Jena (Germany)

Dr. D. H. Scharf
Department of Microbiology and The Children's Hospital
Zhejiang University School of Medicine
Hangzhou, 310058, Zhejiang (P.R. China)
Prof. Dr. A. A. Brakhage, Prof. Dr. C. Hertweck
Faculty of Biological Sciences
Friedrich Schiller University Jena
07743 Jena (Germany)

Supporting information and the ORCID identification number(s) for the author(s) of this article can be found under:
https://doi.org/10.1002/anie.202104372.

© 2021 The Authors. Angewandte Chemie International Edition published by Wiley-VCH GmbH. This is an open access article under the terms of the Creative Commons Attribution Non-Commercial NoDerivs License, which permits use and distribution in any medium, provided the original work is properly cited, the use is non-commercial and no modifications or adaptations are made.

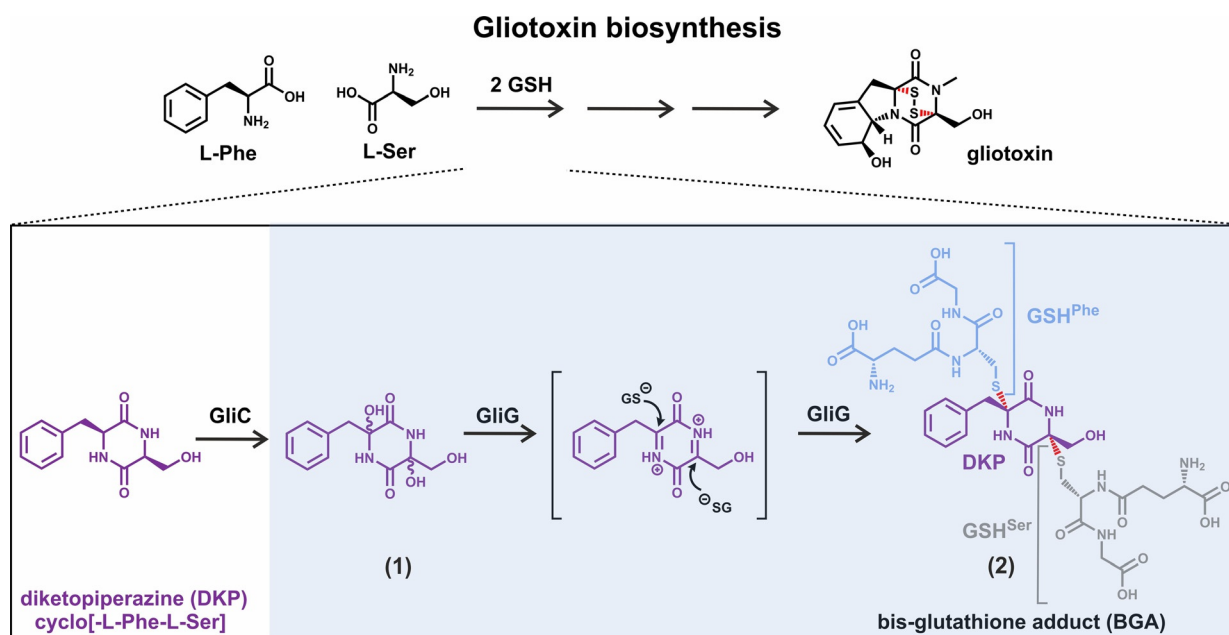


Figure 1. Model for gliotoxin biosynthesis. Enzymatic coupling of the amino acids L-Phe and L-Ser produces the cyclic dipeptide scaffold of gliotoxin.^[5] Upon hydroxylation of the C_α carbons of the diketopiperazine (DKP) ring by the enzyme GliC and water elimination, GliG establishes two carbon–sulfur bonds (red) per DKP with glutathione (GSH) serving as the sulfur donor.^[6a] Referring to their site of attachment at the DKP scaffold, the two GSH molecules are termed GSH^{Phe} (GSH linked to the C_α atom of L-Phe) and GSH^{Ser} (GSH linked to the C_α atom of L-Ser). Stepwise decomposition of the GSH moieties and further downstream processing finally yield the disulfide-bridged gliotoxin.^[7d]

Information).^[6a] To gain insight into its molecular structure, the protein was crystallized, and diffraction data were collected to 2.6 Å resolution (Tables S1 and S2 in the Supporting Information). Due to the low sequence similarity to already solved enzyme structures, selenomethionine labeling was used for phasing. The X-ray structure confirmed the dimeric nature of GliG, however parts of the putative active site (\approx residues 118–146 of helices α 4 and α 5) were disordered (Figure S4A in the Supporting Information). We therefore screened for additional crystallization conditions and eventually identified new parameters at more basic pH (5.5–6.5 compared to 4.7 before, Table S2 in the Supporting Information). These crystals diffracted up to 1.65 Å resolution, and all residues of GliG were fully resolved in the $2F_o - F_c$ electron density map (Table S1 and Figure S4B in the Supporting Information). Dimeric GliG adopts a globular shape with a subunit interface area of about 2073 Å². The monomer folds into the two-domain structure typical of canonical cytosolic GSTs: an N-terminal thioredoxin fold ($\beta\alpha\beta\alpha\beta\alpha$) and a C-terminal domain with six helices (Figure S4 in the Supporting Information).^[10] The subunits are structurally identical (root-mean-square deviation (r.m.s.d.) < 0.26 Å, 174 C_α atoms) and each owns an independent solvent-accessible active site close to the subunit interface. A Dali search highlighted the conserved fold of GliG and listed the bacterial disulfide-bond oxidoreductase YfcG (PDB IDs 5HFK and 3GX0^[11]) as well as fungal GSTs of the Ure2p class (PDB IDs 4F0B,^[12] 4ZBB,^[13] 4ZB8,^[13] 4ZB6^[13] and 1G6W^[14]) as closest structural relatives (Table S3 in the Supporting Information).

Since the substrate of GliG, the bis-hydroxylated diketopiperazine (**1**, Figure 1), was not accessible to isolation or

chemical synthesis in the required amounts, we aimed for a crystal structure in complex with GSH and L-Phe-L-Ser DKP as a surrogate. Although the L-Phe-L-Ser DKP did not bind to GliG, GSH could be trapped in the active site at 1.95 Å resolution (Figure 2A,B and Figure S5A in the Supporting Information). Based on this structure the functional G-site for the binding of GSH to GliG could be assigned.^[15] Like other GSTs, GliG tightly coordinates the γ -Glu of GSH. For instance, Glu82 hydrogen bonds to the α -amino group of the γ -Glu and side as well as main chain atoms of Ser83 coordinate the α -carboxylate (Figure 2B). Ser83 is part of a “STSTL” motif that vaguely reminds of the “SNAIL” consensus sequence used by most GST classes for GSH binding (Figure S6 in the Supporting Information).^[9] In addition, Lys127 of GliG ties the carbonyl oxygen atom of the isopeptide moiety (Figure 2B). The C-terminal Gly residue of GSH is only weakly stabilized by Val18 and Val50, whereas the thiol of GSH undergoes hydrophobic interactions with Val18, Ser24 and Val64. Furthermore, the Cys main chain atoms of GSH form a short anti-parallel β -sheet structure with Val64.^[16] In this respect, the *cis* peptide bond connecting Val64 and Pro65, a hallmark of the thioredoxin fold,^[17] appears to be essential for GSH binding and the overall protein fold.^[18] In agreement, mutation of Pro65 to Ala prevents protein crystallization (Tables S2, S4 and Figure S2B in the Supporting Information) and decreases the thermal stability of GliG by 11 °C as determined by differential scanning fluorimetry (Figure S3B in the Supporting Information).

To evaluate the importance of Glu82, Ser83, Lys127 and other key residues described in the following, we created mutant enzymes (Table S4 and Figure S2B in the Supporting

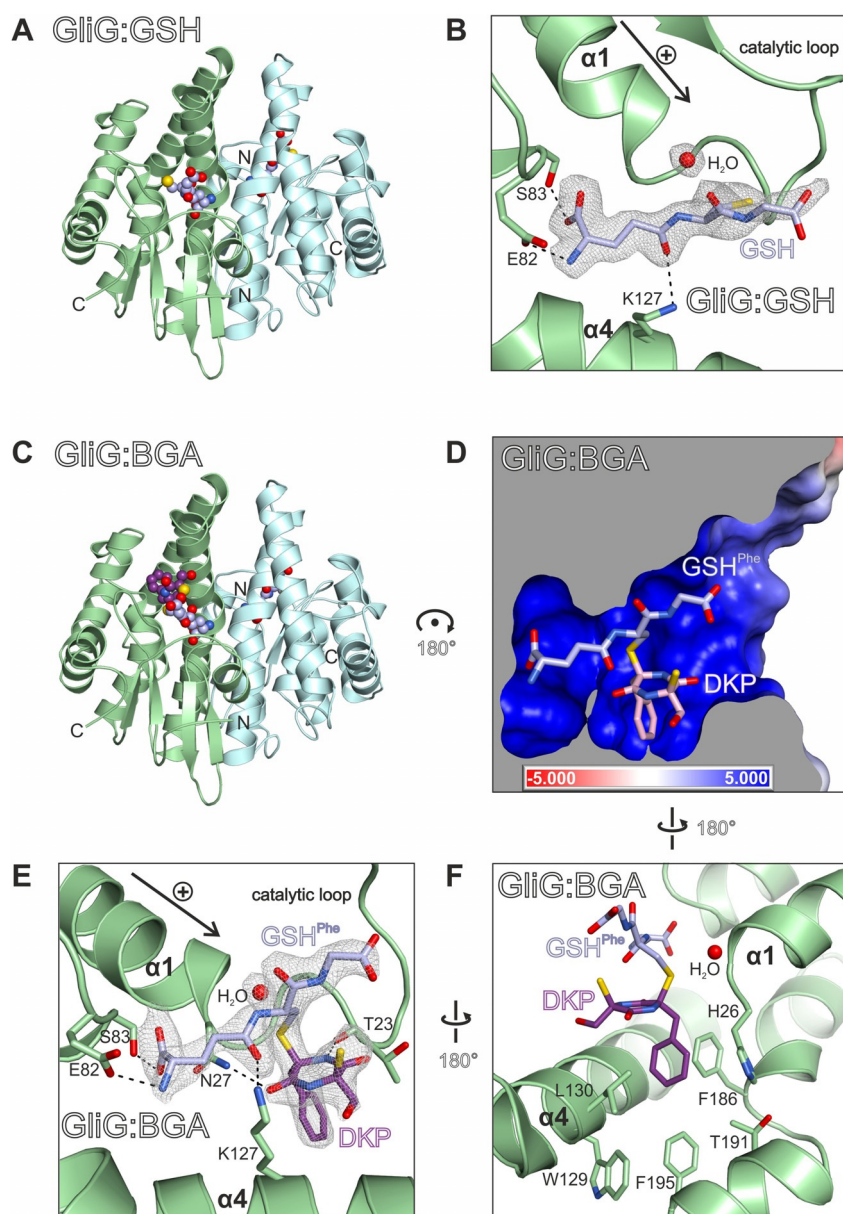


Figure 2. X-ray structures of GliG with bound substrate (GSH) or reaction product (BGA). A) Ribbon illustration of GliG in complex with GSH. The two subunits of the homodimeric assembly are colored green and light blue and their N- as well as C-termini are labeled. The ligand is shown as a multi-colored balls-and-sticks model. Note that the active site of the light blue subunit is hidden in the back of the enzyme. B) $2F_o - F_c$ electron density map for GSH and a water molecule bound to the active site of GliG (gray mesh contoured to 1σ). Key hydrogen bonds between protein residues (shown as sticks and labeled by the one-letter code) and the ligand are illustrated as black dashed lines. The water molecule (red sphere) is located at the positively charged N-terminal end of helix $\alpha 1$. C) Ribbon illustration of GliG bound to BGA according to (A). Carbon atoms of the diketopiperazine moiety of BGA are colored purple, while those originating from GSH are depicted in pale blue. D) Connolly surface representation of the substrate binding cleft of GliG with colors indicating the electrostatic surface potential (see also Figure S5C in the Supporting Information). E) $2F_o - F_c$ electron density map for BGA and a water molecule bound to GliG (gray mesh contoured to 1σ) according to (B). The sulfur atom of the GSH^{Phe} moiety is located closer to the N-terminus of helix $\alpha 1$ than it is the case for the GSH ligand (B). F) Numerous hydrophobic residues line the binding pocket for the Phe side chain of BGA and stabilize the ligand.

Information), and tested their activity. To this end, the crude extract of an *A. fumigatus* ΔgliG strain that accumulates the instable substrate of GliG was incubated with GSH and wild type (WT) or mutant GliG proteins, respectively, and the conversion of the bis-hydroxylated intermediate (1) to the reaction product cyclo[L-Phe-L-Ser]-bis-glutathione adduct (BGA; 2) was monitored by liquid chromatography–high resolution electrospray ionization–mass spectrometry (LC–HRESI–MS, Figure 3A and method section in the Supporting Information). All enzymes are able to catalyze the reaction, but semi-quantitative analysis of product formation indicated differential activities of the enzyme variants (Figure 3B and Figures S12 and S13 in the Supporting Information). In agreement with the structural data, the mutations P65A and K127A have the most severe effect on the catalytic activity of GliG (reduction by more than 80%). The K127R mutant is about 40% less active, suggesting that Arg127 can compensate the function of Lys127 at least to some degree. Similarly, the GliG variants E82Q and E82A show about 85% and 30% residual activity, respectively, as Gln82 and Ser83 can partially take over the function of Glu82 in GSH coordination. The contribution of the Ser83 side chain to GSH binding however is rather low, as revealed by the WT-like activity of the S83A mutant (Figure 3B).

Besides the G-site that is responsible for GSH binding, GSTs feature an H-site for the recognition of their electrophilic substrate.^[15] To localize this H-pocket in GliG, we aimed for structural data with the reaction product BGA. Access to this compound was obtained by blocking GliK, the enzyme acting downstream of GliG in gliotoxin biosynthesis. The corresponding *A. fumigatus* ΔgliK knockout strain^[7d] accumulates BGA and served for its isolation by organic extraction and high-performance liquid chromatography purification (Figure 3C). Subsequent crystal soaking experiments yielded a complex structure at 2.1 Å resolution (Figure 2C–F). In this X-ray structure, the G-site of GliG is occupied by the GSH^{Phe} moiety (GSH molecule attached to the C_α atom of L-Phe of the DKP (Figure 1)), whereas the H-site is taken by the cyclo-

Information), determined their crystal structures up to 1.7 Å resolution (Tables S1, S2 and Figure S11 in the Supporting

dipeptide of the gliotoxin precursor. Due to missing protein interactions, the GSH^{Ser} moiety (GSH molecule attached to

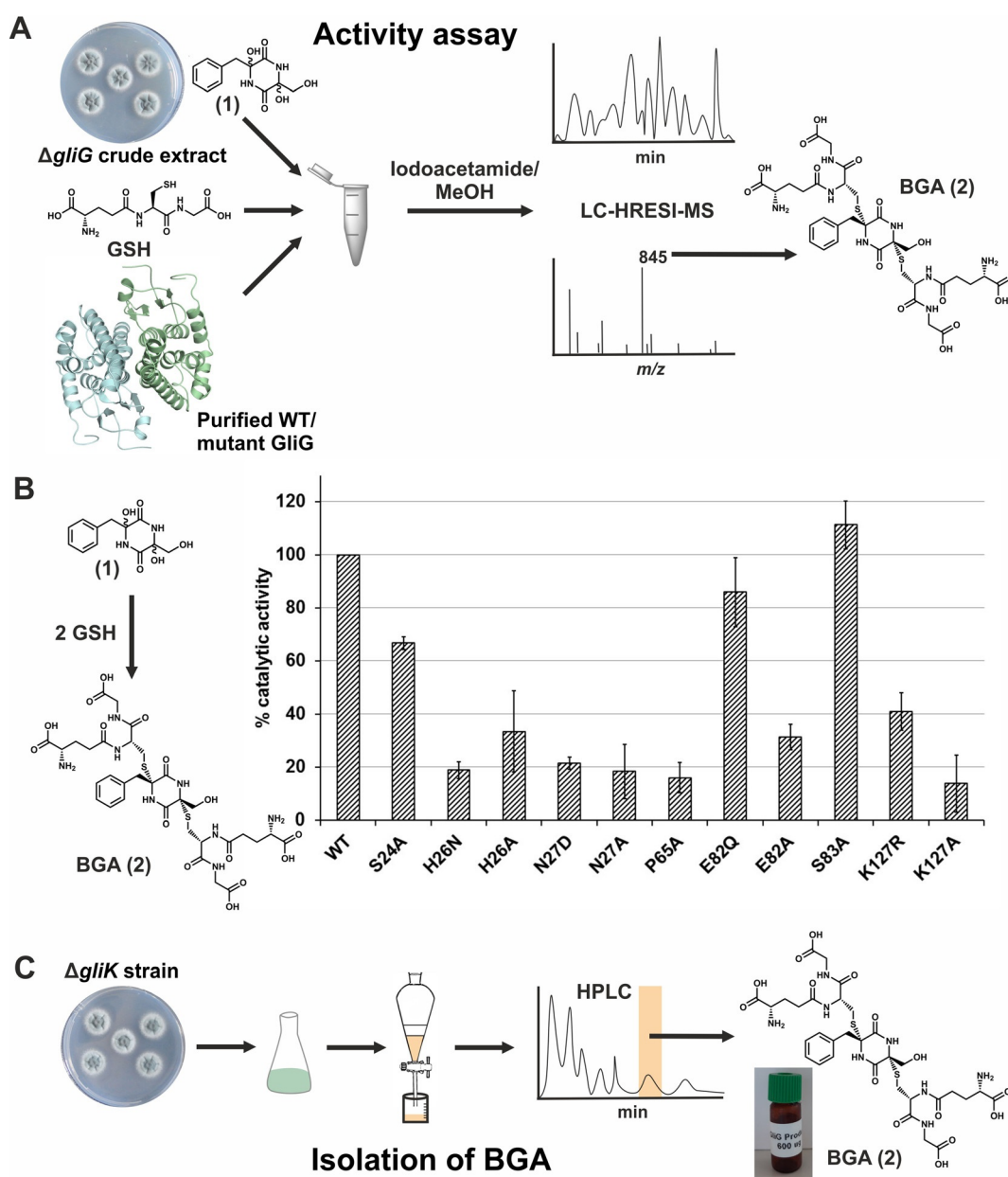


Figure 3. Activity assays and isolation of the reaction product BGA. A) Mixtures of *A. fumigatus* Δ *gliG* crude extract, GSH and purified recombinant WT or mutant GliG protein were analyzed for BGA levels by LC–HRESI–MS to determine the relative activities of GliG variants (see method section in the Supporting Information). B) Semi-quantitative analysis of the activity of GliG variants according to (A). The ratio of the area under the curve (AUC) of the substrate ion (m/z 267 $[M+H]^+$) and the AUC of the product ion (m/z 845 $[M+H]^+$) was calculated. The results are given as the mean \pm standard deviation of three replicates and plotted as percent in relation to WT GliG (100%). See also Figures S12 and S13 in the Supporting Information. C) BGA has been isolated from a genetically modified *A. fumigatus* strain in which the gene encoding GliK, an enzyme that acts after GliG in gliotoxin biosynthesis, has been knocked out.^[7d] The Δ *gliK* strain was cultured and the accumulated BGA was extracted and purified.

the C_{α} atom of L-Ser of the DKP (Figure 1)) is flexible in its conformation and not defined in the $2F_{\text{O}}-F_{\text{C}}$ electron density map (Figure 2E and Figure S5B in the Supporting Information). Notably, the substrate recognition site is largely positively charged due to several surrounding Lys residues (Figure 2D and Figure S5C in the Supporting Information) and appears to be rigid as no conformational changes are observed upon ligand binding. GliG residues 18–26 adopt a loop structure that embraces the ligand and forms a sub-

strate binding pocket (Figure S7 in the Supporting Information). This so-called catalytic loop of GSTs is located C-terminally of the first β -strand of the thioredoxin domain and usually contains the active site residue (see below).^[19] In GliG, the carbonyl oxygen atom of Thr23 (Thr23O) within the catalytic loop hydrogen bonds to the amide nitrogen of the Phe portion of the DKP (Figure 2E and Figure S7B in the Supporting Information). The Phe moiety itself points into a pronounced pocket lined with hydrophobic residues (Thr23,

His26, Trp129, Leu130, Phe186, Thr191, Leu194 and Phe195) and is well stabilized by van der Waals interactions (Figure 2F), while the Ser side chain is not in contact with the protein.

Comparison of the GliG:GSH and GliG:BGA complex structures with its closest relative YfcG in complex with oxidized glutathione (GSSG; PDB ID 3GX0^[11]) highlights some similarities as well as differences in ligand binding. First of all, superposition of GliG:GSH, GliG:BGA and YfcG:GSSG (r.m.s.d. < 1.0 Å, 140 C_α) depicts that the overall binding site for and conformation of the ligands is similar for both enzymes (Figure S8A in the Supporting Information). GSH alone as well as the GSH^{Phe} moiety of BGA bound to GliG roughly align with one of the two identical GSSG halves of YfcG, while the DKP moiety of BGA occupies the binding site for the second GSSG half (Figure S8B in the Supporting Information). GliG probably is unable to bind GSSG or two GSH moieties simultaneously due to steric hindrance with Lys127. By contrast, enzymes with glutathione reductase activity such as YfcG and Ure2p can bind GSSG or two GSH molecules, as they feature a Gly at this position (Figure S8C in the Supporting Information).

To test the impact of Lys127, we created a GliG K127G mutant. X-ray analysis of this variant proved difficult. The mutation K127G appears to increase the flexibility of helix α4, leading to a disordered active site pocket. Crystallization at 4°C with 10 mM GSSG finally allowed us to determine the structure of GliG-K127G:GSSG at 1.5 Å resolution (Table S1 and Figure S8E in the Supporting Information). One GSSG half is fully defined in the 2F_O-F_C electron density map and occupies the same position as observed for GSH or GSH^{Phe} of BGA, while the other GSSG half is only partially visible. Nonetheless, it is obvious that binding of GSSG does not involve the cavity generated by the K127G mutation. Inspection of GliG and YfcG structures indicates that most likely a distinct curvature of helix α4 downsizes the active site cavity of GliG compared to YfcG and prevents binding of GSSG as in YfcG (Figure S8F in the Supporting Information).

Substrate recognition by GliG and YfcG involves the catalytic loop, which is significantly longer in GliG compared to YfcG (Figure S8D in the Supporting Information), and a highly conserved Asn in helix α1. While in YfcG this Asn is hydrogen bridged to the C-terminus of the second GSH monomer (Figure S8C in the Supporting Information), Asn27 of GliG interacts with the cyclodipeptide of BGA, specifically with the carbonyl oxygen atom of the Phe side chain (Figure 2E). Consistently, mutants of Asn27 show about 80% reduction in catalytic activity (Figure 3B). Together the results imply that the amino acid residues required for binding of a second GSH moiety in YfcG/Ure2p proteins have been recruited in GliG for recognition of the DKP scaffold.

Besides evolutionary aspects, the here reported structures of GliG provide insights into the mechanism of glutathionylation during gliotoxin biosynthesis: The two active sites of the GliG dimer are independent and located on opposite sides of the globular particle about 15 Å apart from each other (Figure 2A,C), thus preventing simultaneous modification of a single DKP at both C_α atoms. Furthermore, the fact that

each active site features only one G-site argues for stepwise processing but raises questions about the order of reaction steps. According to the GliG:BGA structure the GSH^{Phe} portion is bound to the active site (Figure 2E and Figure S5B in the Supporting Information). Since the GSH^{Phe} and GSH^{Ser} moieties are structurally identical, this defined orientation has to originate from a preferential stabilization of the DKP. To assess the reason for this favored conformation in more detail, we structurally modelled the GSH^{Ser} portion of the BGA ligand into the active site of GliG by retaining all GSH-protein interactions. In this conformation, the Phe side chain is stabilized by hydrophobic contacts with Met63, and residues of helix α4 (Lys127, Leu130, Tyr131 and Leu135), whereas Ser might hydrogen bond to Thr23O and His26 (Figure S9A,B in the Supporting Information). Mutation of His26 led to a reduction in catalytic activity of about 65–80% (Figure 3B), suggesting that His26 indeed is required for efficient bis-glutathionylation. Compared to the GliG:BGA crystal structure, the hydrophobic cleft for the accommodation of Phe formed by α4 amino acids is rather broad as well as solvent exposed and offers less interaction sites (Figure S9B in the Supporting Information). This model supports the assumption that the crystal structure trapped the preferred conformation of the DKP and that the C_α atom of Phe might be glutathionylated first (Figure 4). Nonetheless, GliG must process also the reverse conformation of the DKP, because otherwise gliotoxin biosynthesis could not be accomplished. Considering the rigidity of the active site pocket, this kind of promiscuity for Phe and Ser side chains could facilitate the production of gliotoxin derivatives in synthetic biology approaches. According to the X-ray structure of GliG, DKPs with residues smaller than Tyr might fit in both orientations in the substrate binding pocket and biotransformation assays with GliC and GliG indeed proved the conversion of non-natural DKPs.^[20]

GSTs usually employ a Ser, Cys or Tyr residue to lower the pK_a value of GSH for the nucleophilic attack of the target molecule.^[9,18–19] Although GliG features a conspicuous Ser24 in the catalytic loop,^[19] it probably is not involved in GSH activation. Distance, orientation and engagement with Lys190 as well as Thr21 main and side chain atoms may prevent any catalytic function (Figure S7A in the Supporting Information). To clarify its potential role in catalysis, Ser24 was mutated to Ala. Our biotransformation assay revealed that the S24A GliG variant retains about 65% of WT catalytic activity, indicating a minor function in catalysis (Figure 3B). For instance, Ser24 could also serve to stabilize the catalytic loop and to restrict its flexibility, thereby shaping the active site pocket. Thus, GliG lacks an obvious catalytic residue—another feature shared with its structural homologs YfcG and Ure2p^[11,21] and supporting the evolutionary relationship with disulfide bond oxidoreductases.

The lack of an active site residue however raises questions about the mechanism of sulfur incorporation. Based on the crystal structures, we here propose the following reaction sequence: GliG binds its bis-hydroxylated substrate (**1**) together with GSH. A hydrogen bond between the Phe-derived amide nitrogen of **1** and Thr23O triggers dehydration (Figure S9C in the Supporting Information). This reaction is

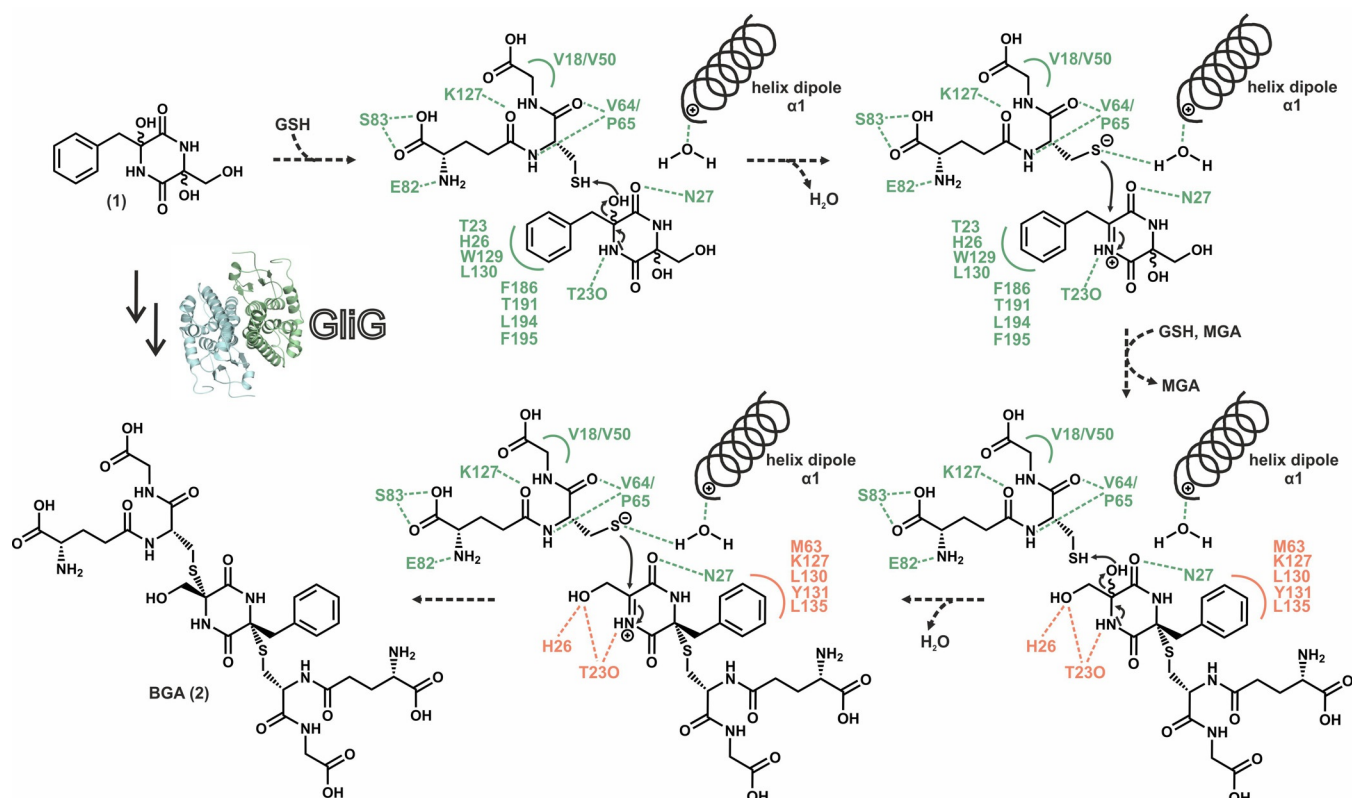


Figure 4. Proposed reaction sequence for GliG. The bis-hydroxylated precursor **1** is converted to the bis-glutathione adduct (BGA, **2**) by the action of GliG (left; solid arrows). The anticipated intermediate steps leading from **1** to **2** are shown on the right (dashed arrows). Interactions with protein side chains (labeled by the one-letter code) are illustrated as half circles (hydrophobic contacts) or dashed lines (hydrogen bonds). Substrate **1** is bound by GliG along with GSH and upon activation by Thr230 eliminates water to yield an imine. Hereby GSH is deprotonated and the resulting sulfur anion, stabilized by the positively charged dipole of helix $\alpha 1$ via a water molecule, nucleophilically attacks the imine intermediate. Based on the crystallographic data, preferential glutathionylation of the Phe moiety is proposed. Once the mono-glutathione adduct (MGA) has been formed, it is released. The final reaction product BGA is yielded by modification of a MGA molecule bound in the reverse orientation (180° rotated).

directly coupled to deprotonation of GSH (Figure 4). The resulting sulfur anion, stabilized by the dipole of helix $\alpha 1$ via a water molecule, nucleophilically attacks the imine intermediate. In support of this mechanism, both GliG:GSH and GliG:BGA structures visualize a water molecule that is hydrogen bonded to Asn27NH (ca. 3.0 Å) at the N-terminus of helix $\alpha 1$ (Figure 2B,E).^[22] Furthermore, the thioether of BGA is aligned with the water molecule and helix $\alpha 1$, while GSH in its protonated form is not (Figure S10 in the Supporting Information). The functional importance of a water molecule stabilized by a helix dipole has also been described for other GSTs.^[18,23] Altogether, the current mechanistic model of GliG-catalyzed glutathionylation and the involved structural features (Figure 4) imply two unimolecular S_N1 reactions—first at the Phe moiety and second at the Ser residue—in which water release from and GSH attack to the DKP occur at the same side of the molecule.

Conclusion

The here reported structural and biochemical results provide insights into the sulfurization step during gliotoxin biosynthesis. The enzyme catalyzing this reaction, GliG, is an

exceptional fungal GST. It employs an electrophilic substrate that is unique among known GST substrates like epoxides, haloalkanes and haloalkenes.^[24] GliG shares low sequence identity to other members of the GST superfamily in *A. fumigatus*,^[6b,25] but has orthologs in numerous ETP producers.^[6a] The data on GliG and the proposed reaction mechanism highlight the functional and mechanistic versatility of GSTs, advance our understanding of C–S bond formation in natural products in general and may inspire enzyme engineering efforts in the future.

Acknowledgements

Financial support by the DFG – SFB 1309 – 325871075 (E.M.H. and M.G.), the Hans-Fischer-Gesellschaft e.V. (E.M.H.) and the Young Scholars' Programme of the Bavarian Academy of Sciences and Humanities (E.M.H.) is acknowledged. We thank Dr. T. Heinekamp (HKI, Department of Molecular and Applied Microbiology) for cultivation of *A. fumigatus*, P. Chankhamjon (HKI, Department of Biomolecular Chemistry) for isolation of the BGA standard and the TUM students F. Adler and D. Frey for experimental support. We are grateful to the staffs of the beamline X06SA

at the Paul-Scherrer-Institute, Swiss Light Source, Villigen, Switzerland and of the beamline ID29 at the European Synchrotron Radiation Facility, Grenoble, France for assistance during data collection and acknowledge funding from the European Community's Seventh Framework Programme (FP7/2007–2013) under BioStruct-X (grant agreement N°283570). Open access funding enabled and organized by Projekt DEAL.

Conflict of interest

The authors declare no conflict of interest.

Keywords: *Aspergillus fumigatus* · carbon–sulfur bond · epipolythiodioxopiperazine · glutathione-S-transferase · mycotoxin

-
- [1] J. P. Latgé, *Clin. Microbiol. Rev.* **1999**, *12*, 310–350.
- [2] a) J. A. Sugui, J. Pardo, Y. C. Chang, K. A. Zarembler, G. Nardone, E. M. Galvez, A. Mullbacher, J. I. Gallin, M. M. Simon, K. J. Kwon-Chung, *Eukaryotic Cell* **2007**, *6*, 1562–1569; b) S. Spikes, R. Xu, C. K. Nguyen, G. Chamilos, D. P. Kontoyiannis, R. H. Jacobson, D. E. Ejzykowicz, L. Y. Chiang, S. G. Filler, G. S. May, *J. Infect. Dis.* **2008**, *197*, 479–486.
- [3] P. Waring, J. Beaver, *Gen. Pharmacol.* **1996**, *27*, 1311–1316.
- [4] D. M. Gardiner, P. Waring, B. J. Howlett, *Microbiology* **2005**, *151*, 1021–1032.
- [5] C. J. Balibar, C. T. Walsh, *Biochemistry* **2006**, *45*, 15029–15038.
- [6] a) D. H. Scharf, N. Remme, A. Habel, P. Chankhamjon, K. Scherlach, T. Heinekamp, P. Hortschansky, A. A. Brakhage, C. Hertweck, *J. Am. Chem. Soc.* **2011**, *133*, 12322–12325; b) C. Davis, S. Carberry, M. Schrettl, I. Singh, J. C. Stephens, S. M. Barry, K. Kavanagh, G. L. Challis, D. Brougham, S. Doyle, *Chem. Biol.* **2011**, *18*, 542–552; c) K. L. Dunbar, D. H. Scharf, A. Litomska, C. Hertweck, *Chem. Rev.* **2017**, *117*, 5521–5577.
- [7] a) M. Schrettl, S. Carberry, K. Kavanagh, H. Haas, G. W. Jones, J. O'Brien, A. Nolan, J. Stephens, O. Fenelon, S. Doyle, *PLoS Pathog.* **2010**, *6*, e1000952; b) D. H. Scharf, N. Remme, T. Heinekamp, P. Hortschansky, A. A. Brakhage, C. Hertweck, *J. Am. Chem. Soc.* **2010**, *132*, 10136–10141; c) D. H. Scharf, P. Chankhamjon, K. Scherlach, T. Heinekamp, M. Roth, A. A. Brakhage, C. Hertweck, *Angew. Chem. Int. Ed.* **2012**, *51*, 10064–10068; *Angew. Chem.* **2012**, *124*, 10211–10215; d) D. H. Scharf, P. Chankhamjon, K. Scherlach, T. Heinekamp, K. Willing, A. A. Brakhage, C. Hertweck, *Angew. Chem. Int. Ed.* **2013**, *52*, 11092–11095; *Angew. Chem.* **2013**, *125*, 11298–11301; e) D. H. Scharf, M. Groll, A. Habel, T. Heinekamp, C. Hertweck, A. A. Brakhage, E. M. Huber, *Angew. Chem. Int. Ed.* **2014**, *53*, 2221–2224; *Angew. Chem.* **2014**, *126*, 2253–2256; f) A. Marion, M. Groll, D. H. Scharf, K. Scherlach, M. Glaser, H. Sievers, M. Schuster, C. Hertweck, A. A. Brakhage, I. Antes, E. M. Huber, *ACS Chem. Biol.* **2017**, *12*, 1874–1882.
- [8] P. Waring, A. Sjaarda, Q. H. Lin, *Biochem. Pharmacol.* **1995**, *49*, 1195–1201.
- [9] D. Sheehan, G. Meade, V. M. Foley, C. A. Dowd, *Biochem. J.* **2001**, *360*, 1–16.
- [10] a) J. D. Hayes, J. U. Flanagan, I. R. Jowsey, *Annu. Rev. Pharmacol. Toxicol.* **2005**, *45*, 51–88; b) H. Dirr, P. Reinemer, R. Huber, *Eur. J. Biochem.* **1994**, *220*, 645–661.
- [11] M. C. Wadington, J. E. Ladner, N. V. Stourman, J. M. Harp, R. N. Armstrong, *Biochemistry* **2009**, *48*, 6559–6561.
- [12] A. Thuillier, T. Roret, F. Favier, E. Gelhaye, J. P. Jacquot, C. Didierjean, M. Morel-Rouhier, *FEBS Lett.* **2013**, *587*, 2125–2130.
- [13] T. Roret, A. Thuillier, F. Favier, E. Gelhaye, C. Didierjean, M. Morel-Rouhier, *Fungal Genet. Biol.* **2015**, *83*, 103–112.
- [14] L. Bousset, H. Belrhali, J. Janin, R. Melki, S. Morera, *Structure* **2001**, *9*, 39–46.
- [15] M. Deponte, *Biochim. Biophys. Acta Gen. Subj.* **2013**, *1830*, 3217–3266.
- [16] P. Reinemer, H. W. Dirr, R. Ladenstein, J. Schaffer, O. Gallay, R. Huber, *EMBO J.* **1991**, *10*, 1997–2005.
- [17] J. L. Martin, *Structure* **1995**, *3*, 245–250.
- [18] R. N. Armstrong, *Chem. Res. Toxicol.* **1997**, *10*, 2–18.
- [19] A. Oakley, *Drug. Metab. Rev.* **2011**, *43*, 138–151.
- [20] D. H. Scharf, J. D. Dworschak, P. Chankhamjon, K. Scherlach, T. Heinekamp, A. A. Brakhage, C. Hertweck, *ACS Chem. Biol.* **2018**, *13*, 2508–2512.
- [21] T. C. Umland, K. L. Taylor, S. Rhee, R. B. Wickner, D. R. Davies, *Proc. Natl. Acad. Sci. USA* **2001**, *98*, 1459–1464.
- [22] a) T. Kortemme, T. E. Creighton, *J. Mol. Biol.* **1995**, *253*, 799–812; b) J. F. Parsons, R. N. Armstrong, *J. Am. Chem. Soc.* **1996**, *118*, 2295–2296.
- [23] X. X. Ma, Y. L. Jiang, Y. X. He, R. Bao, Y. Chen, C. Z. Zhou, *EMBO Rep.* **2009**, *10*, 1320–1326.
- [24] J. Seidegard, G. Ekstrom, *Environ. Health Perspect.* **1997**, *105*, 791–799.
- [25] a) R. A. Cramer, Jr., M. P. Gamcsik, R. M. Brooking, L. K. Najvar, W. R. Kirkpatrick, T. F. Patterson, C. J. Balibar, J. R. Graybill, J. R. Perfect, S. N. Abraham, W. J. Steinbach, *Eukaryotic Cell* **2006**, *5*, 972–980; b) W. C. Nierman, A. Pain, M. J. Anderson, J. R. Wortman, H. S. Kim, J. Arroyo, M. Berriman, K. Abe, D. B. Archer, C. Bermejo, J. Bennett, P. Bowyer, D. Chen, M. Collins, R. Coulson, R. Davies, P. S. Dyer, M. Farman, N. Fedorova, N. Fedorova, T. V. Feldblyum, R. Fischer, N. Fosker, A. Fraser, J. L. Garcia, M. J. Garcia, A. Goble, G. H. Goldman, K. Gomi, S. Griffith-Jones, R. Gwilliam, B. Haas, H. Haas, D. Harris, H. Horiuchi, J. Huang, S. Humphray, J. Jimenez, N. Keller, H. Khouri, K. Kitamoto, T. Kobayashi, S. Konzack, R. Kulkarni, T. Kumagai, A. Lafon, J. P. Latge, W. Li, A. Lord, C. Lu, W. H. Majoros, G. S. May, B. L. Miller, Y. Mohamoud, M. Molina, M. Monod, I. Mouyna, S. Mulligan, L. Murphy, S. O'Neil, I. Paulsen, M. A. Penalva, M. Perlea, C. Price, B. L. Pritchard, M. A. Quail, E. Rabinowitsch, N. Rawlins, M. A. Rajandream, U. Reichard, H. Renault, G. D. Robson, S. Rodriguez de Cordoba, J. M. Rodriguez-Pena, C. M. Ronning, S. Rutter, S. L. Salzberg, M. Sanchez, J. C. Sanchez-Ferrero, D. Saunders, K. Seeger, R. Squares, S. Squares, M. Takeuchi, F. Tekai, G. Turner, C. R. Vazquez de Aldana, J. Weidman, O. White, J. Woodward, J. H. Yu, C. Fraser, J. E. Galagan, K. Asai, M. Machida, N. Hall, B. Barrell, D. W. Denning, *Nature* **2005**, *438*, 1151–1156.

Manuscript received: March 29, 2021

Accepted manuscript online: April 28, 2021

Version of record online: May 14, 2021